PONTIFICIA UNIVERSIDAD CATÓLICA DE CHILE

ESCUELA DE INGENIERÍA

CHALLENGES IN DETERMINING SOIL EVAPORATION FLUXES USING DISTRIBUTED TEMPERATURE SENSING METHODS IN THE PRESENCE OF SHALLOW GROUNDWATER TABLES

MAGDALENA SOFÍA LAGOS DEL RÍO

Thesis submitted to the Office of Research and Graduate Studies in partial fulfillment of the requirements for the Degree of Master of Science in Engineering

Advisor:

JOSÉ FRANCISCO MUÑOZ PARDO

Santiago de Chile, September, 2017

PONTIFICIA UNIVERSIDAD CATOLICA DE CHILE
ESCUELA DE INGENIERIA

CHALLENGES IN DETERMINING SOIL EVAPORATION FLUXES USING DISTRIBUTED TEMPERATURE SENSING METHODS IN THE PRESENCE OF SHALLOW GROUNDWATER TABLES

MAGDALENA SOFÍA LAGOS DEL RÍO

Members of the Committee:

JOSÉ FRANCISCO MUÑOZ PARDO

FRANCISCO SUÁREZ POCH

GUSTAVO CALLE VÁSQUEZ

RODRIGO ALFONSO ESCOBAR MORAGAS

Thesis submitted to the Office of Research and Graduate Studies in partial fulfillment of the requirements for the Degree of Master of Science in Engineering

Santiago de Chile, September, 2017

ACKNOWLEDGEMENTS

I would like to thank God, who gave me the opportunity and gifts that made possible the progress of this investigation.

I thank my advisor, Dr. José Muñoz for his belief in my potentials and for his help in my professional development. I want to give thanks also to Dr. Francisco Suárez, for his unconditional support and all the time he invested in my investigation. Without them and their valuable insights and recommendations, this work couldn't have been possible.

The present work can be seen as a continuation of the work presented in Serna (2015), so I appreciate the assistance of José Luis, the author, in completing the investigation.

I want to thank my family and Phillip for their support and love. Thanks to all my old school and new friends I made during this time, for the good instants and for believing in me; and to my friends of the School of Engineering, for the unrepeatable moments during the career.

I appreciate the help from the Department of Hydraulic and Environmental Engineering, especially Shester and Eduardo.

This research was supported by the scholarship Arturo Cousiño Lyon and CONICYT under the Fondecyt project No. 1170850.

CONTENTS

Page

LIST OF TABLES

Page

LIST OF FIGURES

Page

RESUMEN

La evaporación desde napas someras es un componente importante del balance hídrico de varias regiones. Sin embargo, es un flujo de agua complejo de medir y por lo tanto es importante evaluar nuevos métodos que cuantifiquen este proceso hidrológico. En esta investigación se propone un nuevo método para la determinación de flujos de evaporación desde napas subterráneas someras en base a la combinación del método AHFO (*Actively Heated Fiber Optic* por sus siglas en inglés) y modelación numérica. En este estudio, el método AHFO arrojó estimaciones del perfil de humedad $\theta(z)$ del suelo con una resolución espacial de ~6.5 mm y un error de 0.026 m^3 m^{-3}. El perfil de humedad dado por el modelo numérico resultó ligeramente diferente al perfil medido experimentalmente, donde las mayores diferencias ocurrieron en la superficie del suelo.

Los análisis de sensibilidad e incertidumbre resaltaron que, debido a que las mayores diferencias entre el perfil de contenido de humedad simulado y el determinado experimentalmente ocurren en la superficie, se requiere de una mejor precisión al determinar los parámetros hidrodinámicos del suelo – especialmente para el parámetro *l* de la función de conductividad hidráulica del modelo de van Genuchten-Mualem-. Se concluye además que para mejorar el método propuesto, es necesario incluir las dinámicas de calor-vapor-agua en el suelo. Adicionalmente, se observó que si la calibración de la curva del método AHFO es mejorada, los errores del perfil de humedad estimado se reducirían y de esta manera, estimaciones exitosas de tasas de evaporación para un amplio rango de texturas de suelo pueden ser logradas. De hecho, las escalas espaciales logradas con el método AHFO son una importante ventaja del método propuesto, las que deben ser exploradas para mejorar el análisis del presente trabajo.

Palabras claves: soil evaporation; shallow groundwater tables; distributed temperature sensing (DTS); actively heated fiber optic (AHFO) method.

ABSTRACT

Evaporation from shallow groundwater tables is an important component of the water balance in many regions. However, it is a water flux that is complex to measure; hence, it is important to assess new methods to quantify this hydrological process. In this work, a method is proposed to determine evaporation rates from shallow groundwater tables by combining the actively heated fiber-optic (AHFO) method with numerical modeling. In this study, the AHFO method yielded estimates of the soil moisture (θ) profile with a spatial resolution of ~6.5 mm and with an error of 0.026 m^3 m^{-3}. The numerical model resulted in a slightly different θ profile than the experimentally measured θ profile, where the largest differences occurred at the soil surface.

Sensitivity and uncertainty analyses highlighted that, as the main differences between experimental and simulated θ profiles occurs at the soil surface, a better precision is required when determining the soil hydrodynamic parameters –especially for the *l* parameter of the van Genuchten-Mualem hydraulic conductivity function–. To improve the proposed method, it is also required to include the soil heat-vapor-water dynamics. Additionally, if the AHFO calibration curve is improved, the errors of the estimated θ profile can be reduced and thus, successful estimation of the evaporation rates for a wider range of soil textures can be achieved. In fact, the spatial scales achieved with the AHFO method are an important advantage of the proposed method that should be further explored to improve the analysis presented in this work.

Key words: soil evaporation; shallow groundwater tables; distributed temperature sensing (DTS); actively heated fiber optic (AHFO) method.

1. INTRODUCTION

1.1 Motivation

Arid and semi-arid regions cover approximately 32.4% of the world's land area and are inhabited by more than 1200 million people (MEA, 2005). These regions are defined by their water scarcity, which affects the biomass availability, the agricultural activities, industrial water use and human consumption (Bastidas-Oyanedel et al., 2016). The water scarcity of these regions is expected to worsen due to climate change, through precipitation reduction and increase of global temperatures (IPCC, 2007; Cai et al., 2012). Therefore, to improve water management and environmental protection of these regions under a changing climate, it is important to understand the hydrologic, atmospheric and climatic processes that participate in the water and energy budgets at the atmosphere-vegetation-soil continuum (Assouline et al., 2013; Moene & van Dam, 2014).

Examples of arid regions are the Middle East and North Africa (MENA) region, Australia and Argentina. Northern and central Chile also faces an important challenge in relation to water scarcity, especially in the Copiapó, Huasco and Azapa Valleys, the Pampa del Tamarugal, and in endorheic basins of the Andean Plateau such as the Salar de Atacama (Vásquez et al., 2013; Ortiz et al., 2014) and Salar del Huasco (Hernández-López et al., 2014, 2016). In these regions, groundwater levels typically raise to the soil surface generating shallow saturated zones, from where water evaporates (Hernández-López et al., 2014). Evaporation from shallow groundwater in these regions is an important component of the water balance, and is strongly dependent on the soil moisture (θ) at the first centimeters of the soil profile (Assouline et al., 2013; 2014; Hernández-López et al., 2016).

The assessment of θ has been traditionally realized via the gravimetric method (Klute, 1994), which is a destructive, laborious and time-consuming point-in-space

measurement. Other θ measurement methods have also been developed. Time-domain reflectometry (TDR) is probably the most popular indirect method to determine θ (Topp et al., 1980; Cristi et al., 2016), although it can be expensive when a detailed monitoring network is required or when larger spatial scales are sought (Shuttleworth et al., 2010). The neutron probe infers water content measurements at spatial scales of 1 km, but it cannot provide estimates of θ depths deeper than 0.7 m (Desilets et al., 2010), which is of interest when investigating the vadose zone. Thermal methods have been widely used in vadose zone hydrology (Campbell et al., 1991; Li et al., 2016). In the last years, distributed temperature sensing methods using fiber-optic cables (FO-DTS) have gained ground among researches, and have been used indirectly to determine water fluxes and θ in the subsoil from thermal measurements (Sayde et al., 2010, 2014; Steele-Dunne et al., 2010; Ciocca et al., 2012; Striegl & Loheide, 2012; Benitez-Buelga et al., 2014; 2016; Dong et al., 2015; 2016).

Distributed temperature sensing (DTS) is based on the light's reflection within an optical fiber for the temperature determination along the fiber-optic cable, with spatial resolution of 0.25-1.0 m, temporal resolution of 1-60 s, and an accuracy of ± 0.01 °C, along cables up to 10 km long (Hausner et al., 2011; Suárez et al., 2011a). This technology enables monitoring temperature at large extensions, offering an alternative for continuous measurements at a wide range of spatial scales in the area of interest. To quantify θ using DTS with a high accuracy, two methods have been proposed: the passive and the actively heated fiber-optic (AHFO) methods (Steele-Dunne et al., 2010; Sayde et al., 2010). Here, there is a focus on the AHFO method as it does not depend on the meteorological conditions of the area of interest. The AHFO method requires use of metallic elements in the fiber-optic cable (electrical conductors), where an electric potential is used to heat the cable, and its thermal response is related to θ (Serna et al., 2017). Sayde et al. (2010) demonstrated that the θ can be quantified with a precision of ~10% of the measurement, and later performed field campaigns in an agricultural field subjected to irrigation to determine the θ and the water fluxes near the soil's surface. Ciocca et al. (2012) applied the AHFO method in a lysimeter filled with a loamy soil. In

their experiments, the heating and the cooling phases were used to determine the soil thermal conductivity and heat capacity, from which they estimated the θ profile. Striegl and Loheide (2012) used the AHFO method under field conditions, and related the temperature increase (ΔT) with the θ. The advantage of using the AHFO method is that it only requires a cable, which allows a heat pulse application and an energy dissipation monitoring. Also, the method involves one temperature calibration for the cable, instead of multiple calibrations for each of the temperature sensors. Finally, the spatial scale achieved by the FO-DTS methods allows studying hydrological phenomena occurring from centimeters to kilometers, which opens a new perspective to the understanding of the environmental physical processes.

A deep comprehension of the evaporation dynamics and its spatial and temporal variability are a key element in the understanding of hydrological processes; hence, it is important to accurately assess this variable for water resources, climate change and hydrological purposes. Several techniques exist for evaporation assessment, including lysimeters (Marek et al., 2016), scintillometers (McJannet et al., 2011), eddy covariance systems (Scott, 2010) and the DTS-based Bowen ratio (BR-DTS) method (Luxemburg et al., 2013). All of these techniques involve inherent advantages and limitations that need taking into account. With the aim of investigating new measurement techniques to quantify soil evaporation, this study explores the applicability and challenges associated to the use of the AHFO method to determine the θ profile, and to use this information to estimate the evaporation fluxes from soils with shallow groundwater tables, where the vadose zone is hydraulically connected between the soil surface and the groundwater level. Because it is the first time that the AHFO method is being used to investigate if evaporation rates can be determined, for simplicity, experiments were designed where the vapor pressure gradient and the flow due to thermal gradients within the soil profile are negligible (Nasrallah & Perre, 1988; Prat, 2002).

1.2 Hypothesis

The hypothesis of this study is that the determination of soil evaporation fluxes is possible by combining the distributed temperature sensing (DTS) method through a fiber optic cable and the vadose zone theory in the presence of shallow groundwater tables.

1.3 Objectives

The overall objective of this investigation is to assess a proposed method based on measurements by the distributed temperature sensing DTS with fiber optic cables for the determination of soil evaporation fluxes in presence of groundwater tables. The following are the specific objectives:

1) To build an experimental installation that allows the active method assessment and the water content determination through the DTS method. The installation consists in a sandy-soil column, 1.5 m tall, connected to a DTS and a constant-head reservoir that maintains a constant water table.

2) To build active method's calibration curves for a sandy soil, considering the heat pulse duration and the optimal integration time of the soil's thermal response.

3) Through the active method, to obtain the water content profile for the soil column in steady state and for a water table at 1.2 m depth.

4) To determine the evaporation rate through inverse modelling and a sensitive analysis, based on numerical modelling (HYDRUS-1D)

5) Based on Monte Carlo Simulations, to explore the hydraulic properties parameter's space of the soil to understand the complex relationship between all parameters.

1.4 Structure of the thesis

This thesis is organized in the following way. Chapter 1 is a brief introduction to the topic that shows the motivation of this work, hypothesis and the general and specific objectives of the thesis. Chapter 2 consists in the materials and methods applied to this study. The explanation of how the soil properties were assessed is presented, as well the DTS and active method theory and details of the experimental set-up and numerical modelling. Chapter 3 is a presentation of results and discussion about the soil properties, distributed water content measurements by the DTS and active method and the results of the evaporation rate estimation in base of the previous obtained data. Finally, chapter 4 corresponds to the conclusions and perspectives that can be drawn from the work reported previously.

2. MATERIALS AND METHODS

In this section, the theory, experimental and numerical methods are described, which are used to determine the soil's properties, its performance regarding to heat pulses and to determine the water content profile and predict the related evaporation rates of the soil in the presence of shallow groundwater tables.

1.5 Physical and Hydrodynamic properties of the soil

The particle-size distribution of the soil used in this study was determined by sieving (Klute, 1994), and was utilized to estimate the texture, and the uniformity (C_u) and curvature (C_c) coefficients (Klute, 1994). The soil particle density (ρ_s) was estimated using the pycnometer technique (ASTM D 854-91; Klute, 1994).

The water retention curve, $\theta(h)$ or WRC, and the hydraulic conductivity function, K (h) or HCF, are two key properties that control water flow in a variably saturated medium (Campbell, 2013; Sandoval et al., 2017).

The WRC, which describes the relationship between the pressure head, h, and the volumetric water content, θ, represents the soil's capacity of retaining water. The WRC was described using the van Genuchten (1980) model:

$$\theta(h) = \frac{\theta_s - \theta_r}{(1 + |\alpha h|^n)^m} + \theta_r \tag{2.1}$$

where θ_r and θ_s are the soil saturated and residual volumetric water contents, respectively; α is the inverse of the air-entry pressure; and n and m are empirical parameters resulting from best-fit procedures to data related to the pore size distribution, where typically $m = 1 - 1/n$ with $n > 1$ (Shokri & Salvucci, 2011). In this work, the WRC was experimentally determined using the simplified evaporation method (Peters & Durner, 2008).

In the evaporation method, a soil sample is subjected to evaporation under laboratory conditions, while the pressure head and the sample weight are registered. The WRC is constructed using the relationship between sample weight and the volumetric water content of the sample (Peters & Durner, 2008). The HYPROP device (UMS) was employed to implement the evaporation method. Soil cores were inserted into 250-cm^3 stainless steel cylinders (8-cm diameter and 5-cm height). The sample is let to capillary saturate by placing it in a 4.9-cm depth water reservoir. Two tensiometers (accuracy of ± 2.5 hPa and resolution of ± 0.05 hPa) were inserted at depths of 1.25 and 3.75 cm, and the bottom of the substrate core was sealed. Each substrate core was installed on top of the weighing plate of a 0.01-g precision balance. The experimental retention data were then used to fit the WRC parameters of the van Genuchten (1980) model to the experimental data.

The HCF, which represents the ease with which water moves through a porous media, was described using Mualem's model (Assouline & Or, 2013):

$$K(h) = K_s Se^{l}\left[1 - \left(1 - S_e^{1/m}\right)^{m}\right]^2 \tag{2.2}$$

where K_s is the saturated hydraulic conductivity; $S_e = (\theta - \theta_r)/(\theta_s - \theta_r)$ is the effective saturation; and l is the pore-connectivity parameter, which is typically assumed to be 0.5 (Mualem, 1976). The required parameters to describe the HCF are those obtained by the fitting of the van Genuchten (1980) WRC model to the experimental water retention data combined with the K_s. In this study, the K_s was estimated with the KSAT apparatus (UMS), which is a falling-head permeameter that uses the same soil cores as the HYPROP device.

1.6 Determination of distributed soil moisture using the AHFO method

Heat pulse methods have been widely used for the assessment of soil's thermal properties, θ, and water movement in soils (Campbell et al., 1991; Bristow et al., 1994; Tarara et al., 1997). Laboratory and field studies indicate that these methods offer advantages such as low cost, low soil disturbance and automatic and frequent measurements. However, these methods typically deliver a point-in-space measure (Ren et al., 2003).

The AHFO method is an approach that has been successfully used to observe spatially distributed subsurface water movement. Previous studies have demonstrated the feasibility of using AHFO for accurate distributed measurement of soil moisture in soil columns or lysimeters (Sayde et al., 2010; Ciocca et al., 2012), and for successful measurement of soil moisture and water fluxes at field scales between 0.29 and 1,000 m (Sayde et al., 2014; Benítez-Buelga et al., 2016).

The AHFO method empirically correlates θ and the soil's thermal response to a heat pulse generated along a fiber-optic cable. Sayde et al. (2010) proposed to quantify the soil's thermal response using a parameter named cumulative temperature, T_{cum}:

$$T_{cum} = \int_0^{t_0} \Delta T(t)\, dt \tag{2.3}$$

where $\Delta T(t) = T(t) - T(t = 0)$ is the temperature difference in a specific position of the cable between time t and the time when the heat pulse is first applied ($t = 0$), and t_0 is the total integration time, which can be different than the heat pulse duration, t_f (Serna et al., 2017).

The reason to quantify the soil's thermal response by means of the T_{cum} is that the latter depends on the properties of the media. To generate a heat pulse, an electric current I is circulated through a fiber-optic cable, which contains conductive elements (e.g., copper and/or steel filaments) and an electrical resistance, $R(T)$, which depends on

the cable's temperature, *T*. When an electrical current flow through the cable, the heat dissipated along the cable, Q_H, can be estimated using the Joule heating law (Griffiths, 2008; Serna, 2015):

$$Q_H = Pt = R(T)I(t)^2 t \tag{2.4}$$

where *t* (s) is the duration of the heat pulse. This energy dissipates as heat in the cable as well as the surrounding environment. Assuming that the cable and the environment have a specific heat capacity, C_p, which depends on the temperatures of the media, the water content and the soil's structure; the heat dissipation in the cable/soil system can be calculated as (Mills, 1999):

$$dQ_H = C_p dT \tag{2.5}$$

Equation (2.5) can be integrated and equated to the heat dissipated along the cable (Eq. 2.4). To achieve this, it is necessary to know how the heat capacity depends on the temperature. If it is assumed that the heat capacity is constant, it is possible to find the temperature increase in the cable's surroundings and to determine the T_{cum}:

$$T_{cum} = \int_0^{t_0} \Delta T(t)\, dt \approx \int_0^{t_0} \frac{R(T)I(t)^2}{C_p} t\, dt \tag{2.6}$$

Despite Eq. (2.6) is not exact because it was assumed that the heat capacity is independent of the temperature, it allows understanding the processes influencing the temperature rise in the cable's surroundings for each of its segments. The temperature increase depends on the thermal properties of the soil (which are function of θ and the soil structure), the electric properties of the conductor elements and the electrical current flowing through the cable. Moreover, it can be concluded that the temperature increase in each cable's segment and surroundings is proportional to the electrical resistance of the fiber-optic cable, to the square of the electrical current, and is inversely proportional to the heat capacity of the cable/soil system. From Eq. (2.6) and knowing that the heat capacity of the unsaturated porous media increases with θ (Jury & Horton, 2004), it can

be inferred that θ increases as T_{cum} decreases. Nevertheless, Eq. (2.6) has little practical application: as the heat energy dissipates during the heat pulse, the thermal boundary layer at the cable's surroundings grows and, therefore, the thermal properties change as a function of the temperature shifts. This process hampers the estimation of the heat capacity of the cable/soil system.

Equation (2.6) is complex to solve analytically or numerically, but one can take advantage of FO-DTS systems since they provide temperature estimates along the fiber-optic cables, which are influenced by the thermoelectric properties of the cable as well as by the thermal properties of the soil. Hence, it is possible to use the measured DTS temperatures to directly calculate T_{cum} using Eq. (2.3). Moreover, since FO-DTS instruments count cumulative photons, the standard deviation of T_{cum} decreases with the square root of the integration interval (Selker et al., 2006a; Sayde et al., 2010). Therefore, in each cable segment it is possible to correlate T_{cum} with θ if independent measurements of the latter are registered.

Sayde et al. (2010) proposed an empirical exponential curve for each soil to relate T_{cum} and θ. This curve can be obtained from laboratory conditions and extrapolated to field conditions (Sayde et al., 2014). Mathematically, the correlation between T_{cum} and θ can be made using any expression that predicts a decrease of T_{cum} as θ increases (as described before). In the present study, the following potential expression was used (Serna et al., 2017):

$$\theta = \begin{cases} \theta_r & aT_{cum}{}^{b} \leq \theta_r \\ aT_{cum}{}^{b} & \theta_r < aT_{cum}{}^{b} < \theta_s \\ \theta_s & aT_{cum}{}^{b} \geq \theta_s \end{cases} \tag{2.7}$$

where *a* and *b* are empirical fitting parameters; and θ_r and θ_s are inferred from the soil's WRC. To find the empirical parameters of Eq. (2.7), i.e., *a* y *b*, the square error between the θ estimations and an independent measurement of θ must be minimized. Even when

Eq. (2.7) is still an empirical relation, the inclusion of the hydrodynamic properties provides a physical constrain on the estimated θ (Serna et al., 2017).

Serna et al. (2017) present a detailed assessment of the AFHO method, where they developed the calibration curves (Eq. 2.7) that are used to determine θ for different hydraulic conditions, i.e., different water table depths, at steady state regime; and for different heat pulse durations. In the present work, the groundwater table was fixed at the same depth than that used by Serna et al. (2017), and their calibration curves were used to determine the soil moisture profile through the AHFO method, and to investigate the feasibility of using AHFO to determine soil evaporation fluxes. As suggested by Serna et al. (2017), 20-min heat pulses (at ~17.5 A and ~2.4 W m^{-1}) were used. This duration and power make temperature changes easier to read and less susceptible to temperature drift errors (Serna, 2015), and should not result in water movement out of the measuring region or in free convection in liquids (Bristow et al., 1994). Nonetheless, it is conservative to be aware that the results may perturb the thermal and hydraulic conditions in the media. For this reason, the analysis presented in this work is valid for the hydraulic steady state regime prior to the application of the heat pulse.

1.7 Determination of evaporation fluxes using numerical modeling

The process of evaporation involves transport of liquid, water vapor and heat (de Vries, 1958; Parlange et al., 1998; Prat, 2002). According to Assouline et al. (2013), there are two relevant mechanisms in the presence of shallow groundwater tables: evaporation at the soil surface sustained by the hydraulic connectivity from the groundwater table up to the surface, and subsurface evaporation maintained by diffusive vapor removal through the porous medium. The second mechanism was neglected because in the experiments the vapor pressure gradient was negligible. Therefore, the water movement in a variably saturated porous media was described using the following one-dimensional version of the Richards (1931) equation:

$$C\frac{\partial h}{\partial t} = \frac{\partial}{\partial z}\left[K\left(\frac{\partial h}{\partial z} + 1\right)\right] \quad (2.8)$$

where $C = \partial\theta/\partial h$ is a function describing the saturation rate of change with respect to the matric head, t is time, and z is the vertical spatial coordinate (positive upwards). The unsaturated soil hydrodynamic properties, i.e., the WRC and the HCF, which are highly nonlinear functions of h, are required to solve the Richards (1931) equation. Eq. (2.8) assumes that there is hydraulic connectivity from the groundwater table up to the soil surface, that the air phase plays no significant role in the liquid flow processes, and that the flow due to thermal gradients is negligible (Šimůnek et al., 2016). These assumptions are supported by the fact that the effect of gaseous pressure is relevant only in cases of drying at high temperature and where the initial moisture content is rather weak (Nasrallah & Perre, 1988), and because the transport of energy can be neglected at situations where drying rates are sufficiently low for not imparting significant temperature gradients within the soil (Prat, 2002).

The resolution of Eq. (2.8) was performed using the HYDRUS-1D software (Šimůnek et al., 2016), which numerically solves the Richards' (1931) equation. HYDRUS-1D deals with different boundary conditions such as boundaries controlled by atmospheric conditions, free drainage and prescribed head and flux boundaries. As described below, the conditions observed in the experiments were used to define the boundary conditions of the simulations. In particular, it was investigated if the evaporation fluxes can be inferred from the θ profile estimated using the AHFO method.

Figure 2-1 presents a conceptual diagram that explains the methodology followed in this research. A vertical high-resolution DTS pole is inserted into the soil (I). This DTS system allows measuring soil temperatures at high spatial and temporal resolutions (II). A heat pulse is applied in the DTS pole using an electrical system, and the increase in temperatures (ΔT) is registered at different depths (III). At a depth z^*, the ΔT is then used to calculate T_{cum} (z^*) using Eq. (2.3) (IV). Then, the θ at a depth z^* is estimated using Eq. (2.7). This process is repeated for all the depths and yields the θ profile in the

soil (V). Finally, the soil hydrodynamic properties and the θ profile are used as input data to numerically solve the Richards (1931) equation. An inverse modeling exercise allows finding the evaporation rate (VI) when matching the observed and simulated θ profiles.

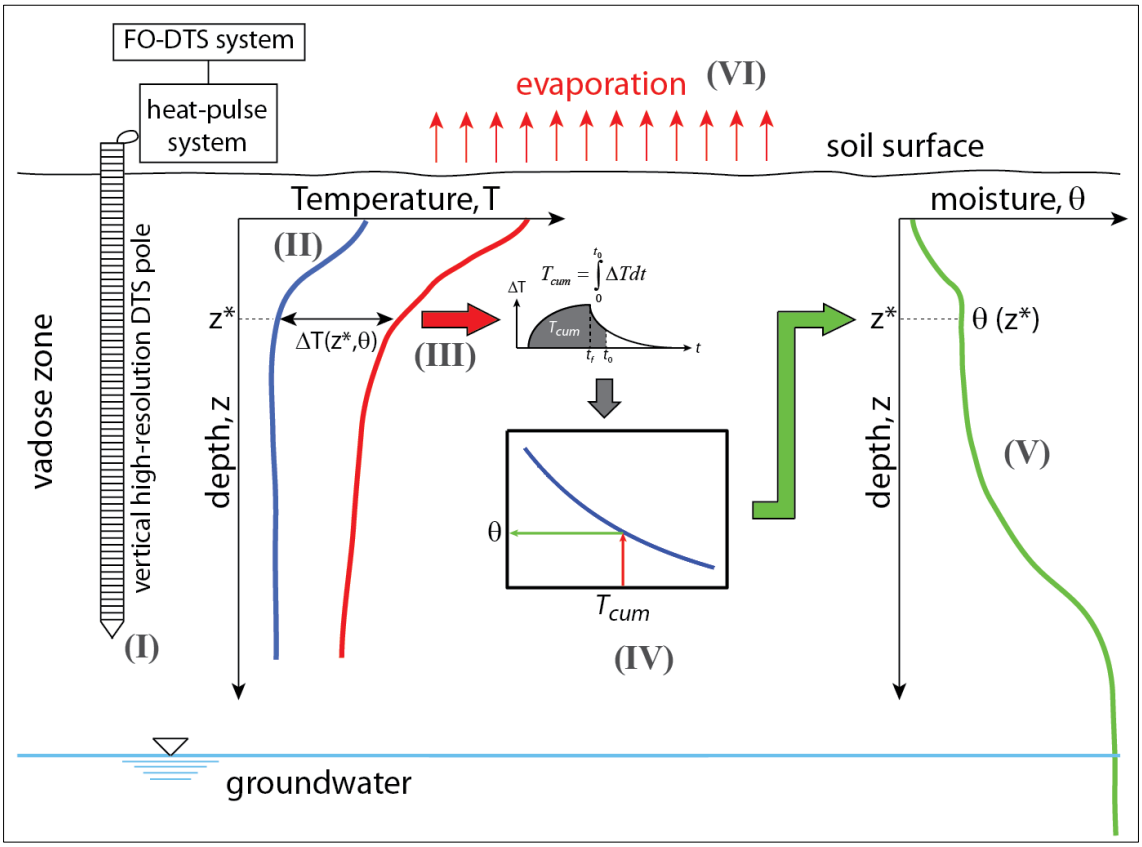

Figure 2-1: Conceptual model of the proposed methodology. The AHFO method is used to infer the experimental moisture profile from the FO-DTS measurements in the DTS pole. Then, numerical simulations are used to determine the evaporation rates that results in an agreement between the experimental and simulated θ profile.

1.8 Experimental setup

An experimental setup was built to investigate if θ and soil evaporation fluxes can be determined using the AHFO method combined with numerical modeling. The experimental setup consists in: 1) a soil column with moisture sensors and a system that

allows fixing the water table at different depths and measuring the soil evaporation rates; 2) a FO-DTS measurement system with a high-vertical resolution, which has a fiber-optic cable with metallic conductive elements; and 3) an electric system which allows a current intensity to flow through an electric circuit, i.e., the fiber-optic cable. The following sections detail each of the components of the experimental setup, which is depicted in Figure 2-2.

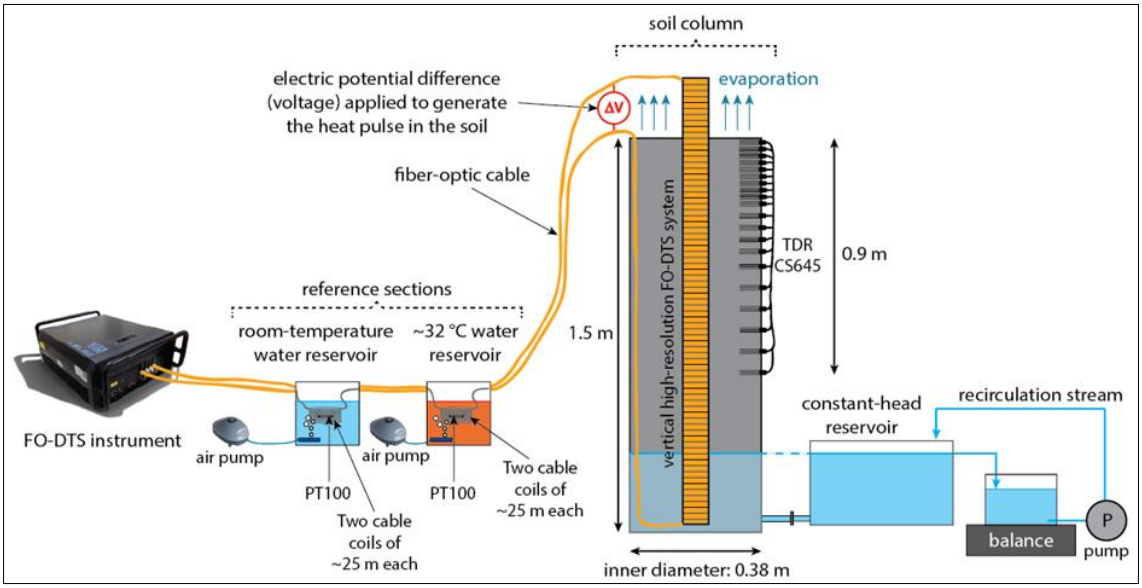

Figure 2-2: The experimental setup is comprised by the FO-DTS instrument, the reference sections, the fiber-optic cable layout in the experimental setup, the soil column the location where the voltage (ΔV) is applied to generate the heat pulse within the soil column, the constant-head reservoir, and the recirculation system that allow fixing the depth of the groundwater table and measuring the evaporation rate.

1.8.1 Experimental soil column

A 0.38 m inner diameter and 1.50 m long soil column was used in the experiments. At its upper 0.90 m, 20 time-domain reflectometry (TDR) soil moisture sensors were mounted (TDR CS-645, Campbell Sci. Logan, UT), as shown in Figure 2-2. The vertical spacing between the sensors is variable, being 0.025 m from the

column's surface to 0.25 m depth; 0.05 m between 0.25 m and 0.50 m depth; and 0.08 m between 0.50 m and 0.90 m depth. The soil moisture sensors were connected to a datalogger (CR1000, Campbell Sci., Logan, UT) that collected data at intervals of 5 min. A vertical high-resolution FO-DTS system, similar to that presented by Suárez et al. (2011a), was installed inside the soil column. As described in the next section, the FO-DTS system allows performing the AHFO method to determine the spatial distribution of θ.

The filling of the experimental column was performed carefully to try to achieve a uniform soil profile in terms of compaction and density. The column was filled with layers of ~0.30 m thickness. Each layer was compacted in a similar way until filling completely the soil column. This filling methodology allowed obtaining an average soil's density of 1400 kg m^{-3}.

The water table within the column can be fixed at any depth between 0.2 and 1.3 m by means of a water reservoir connected to the bottom of the soil column (Figure 2-2). This reservoir has an outlet that allows fixing the water level in it. The water that exits in this reservoir goes into another reservoir that is continuously weighed using a balance (Midrics 1 MW2PU1-15DC-L, Sartorius AG, Germany). A pump recirculates water between these two reservoirs. Because the only water loss of the system occurs at the soil column surface, the weight reduction measured at the balance corresponds to the mass of water evaporated in the soil. Hence, the evaporation rates can be measured. As a reference, similar systems used to measure evaporation rates from water bodies enabled evaporation estimates with errors on the order of ± 0.1 mm d^{-1} (Ruskowitz et al., 2014; Silva et al., 2017).

A vertical high-resolution FO-DTS system was installed inside the experimental column prior to filling it with soil. This system consists in a fiber-optic cable (DNS-3454, AFL Telecommunications, Spartanburg, SC), two reference sections, and a DTS instrument (Ultima-XT DTS, Silixa, Hertfordshire, England), as shown in Figure 2-2.

The fiber-optic cable is a loose-tube steel conduit of 2 mm diameter. The steel conduit, at the same time, is covered by six steel filaments and six copper filaments, each of 0.6 mm diameter. The metal components of the fiber-optic cables were used as an electrical resistance heater; therefore, they enable the application of the AHFO method. A polyethylene cladding covers the filaments and protects the cable.

One hundred and forty meters of the fiber-optic cable were wounded in a helicoidally way around a PVC pipe (0.11 m diameter and 1.80 m tall) that was used as a support. The interior of the PVC pipe was thermally insulated using a polyurethane foam. This system, similar to those used by Selker et al. (2006b) and Suárez et al. (2011a), allows having a spatial resolution of ~6.5 mm (sampling resolution of ~3.2 mm). The vertical high-resolution FO-DTS system was installed at the center of the experimental column until a depth of 1.47 m (Figure 2-2).

Two reference sections were included in the experimental setup to calibrate the FO-DTS system (Figure 2-2). The first section corresponded to a room-temperature water reservoir, and the second section was a water reservoir at ~32 °C. Both reference sections were stirred by air pumps (SE-303, Guangdong Boyu Group Co., Ltd., Chaozhou, China) operating at a flow rate of 3.5 L min^{-1} with the aim of achieving a uniform temperature in the reference baths. The reference sections were monitored by 100 Ω platinum resistance thermometers (PT100, Silixa, Hertfordshire, England), which allowed calibration of the temperature profiles along the cable, and evaluation of the precision and accuracy of the DTS measurements. According to the manufacturers' specifications, the platinum resistance thermometers have an accuracy of ± 0.1 °C and a precision of ± 0.02 °C.

The fiber-optic cable was connected to the FO-DTS instrument, which according to the manufacturer's specifications, has a resolution of less than 0.1 °C (at integration intervals of 3 minutes), and a monitoring spatial resolution of 0.25 m.

The FO-DTS measuring system enables using the duplex single-ended and double-ended configurations (Hausner et al., 2011). In this work, since the cables are

relatively short (< 1 km), the duplex single-ended configuration was selected (Hausner et al., 2011; Suárez et al., 2011b; Hausner & Kobs, 2016). The assessment of accuracy and precision of the DTS measurements –based on the mean bias (*MB*) and root mean square error (*RMSE*)– was performed using a computational software provided by the Center for Transformative Environmental Programs (CTEMPs). This software is coded in Matlab® and also allows calibration of the DTS temperatures using the algorithms presented by Hausner et al. (2011) through a graphical user interface.

1.8.2 Electric system

An electric current controller system similar to that presented by Kurth et al. (2013) was built. This controller enables application of the heat pulses along the fiber-optic cables and thus, to use the AHFO method to determine θ. The main features of the electric system are: 1) it has a dimmer that controls the electric current flow through the system; 2) it has a digital multimeter for registering the actual current flowing through the fiber-optic cable and the existing voltage between both ends of the electrical circuit; 3) it has a timer that enables fixing the current pulses duration; and 4) it has a programmable logic controller (Weintek Labs., Inc. Taiwan), which permits automatic control of the system. The specific details of the electrical system are presented elsewhere (Serna, 2015).

1.9 Soil column experiments and conditions of the numerical model

Similarly than the work of Serna et al. (2017), in the experiments the groundwater table was fixed at a depth of 1.2 m, and a fan was installed above the soil column to generate a wind current of ~1-2 m s^{-1}. This configuration resulted in an evaporation rate of 2.2 m d^{-1}. Three repetitions were performed at the hydraulic conditions tested in the experiments, which were performed at steady state. Before applying the 20-min heat pulse, the soil's initial temperature profile was established as the mean temperature during the 5 min before applying the heat pulse, as recommended by Sayde et al. (2010). After the heat pulse application, the temperatures in the soil profile were still registered until they returned to its initial condition. Once this condition

was reached, the next repetition was carried out. All the FO-DTS measurements were performed with a vertical spatial resolution of ~6.5 mm and a temporal resolution of 5 s. In each experience, the temperatures determined by the FO-DTS system were dynamically calibrated in base of the measured temperatures at the reference sections. The calibrations were made through the explicit calculation of parameters method using three reference sections, whereas the fourth reference section was used to assess accuracy and precision of the DTS measurements (Hausner et al., 2011).

A soil domain of 1.5 m long with a discretization of 5 mm was used in the numerical model. The evaporation rate measured in the laboratory was used as top boundary condition, whereas the bottom boundary condition was prescribed using a fixed pressure head according to the depth of the groundwater table. The initial conditions of the simulations consisted in an equilibrium profile for the pressure head, although it should be pointed out that because the experiments were performed at steady state regime, the initial conditions do not alter the resulting steady state θ profile. The simulations were run in transient mode until steady state was reached, and all the simulation results are presented for the steady state.

3. RESULTS AND DISCUSSION

1.10 Physical and hydrodynamic soil properties

The soil used in this research had 96% sand, 2% silt, and 2% clay; with C_u = 2.7, C_c = 1.2, d_{50} = 0.14 mm and ρ_s = 2,730 kg m^{-3}. The low values of C_u and C_c indicate that the soil particle-size distribution is highly uniform. Hence, the soil can be classified as a sand (USDA, 2014).

Figure 3-1 shows the soil WRC and HCF, and the fitted parameters of the van Genuchten-Mualem's hydraulic model estimated from the laboratory measurements. The van Genuchten model (1980) provided a good fit to the WRC data (r^2 = 0.99) and allows determining that soil moisture ranges between 0.146 and 0.458 m^3 m^{-3}. This range of soil moisture is used to bracket the limits of the relationship between T_{cum} and θ (Eq. 2.7). The resulting hydrodynamic parameters are also within the expected values for sands (Rawls et al., 1982; Twarakavi et al., 2010).

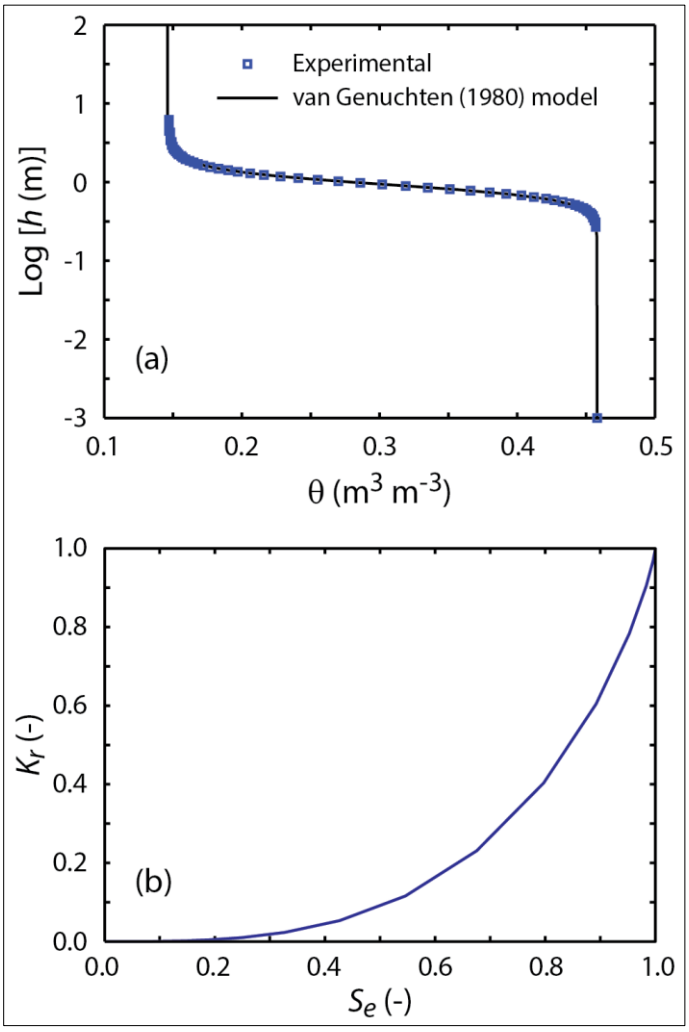

Figure 3-1: Soil hydrodynamic properties: (a) water retention curve; (b) relative hydraulic conductivity function ($K_r = K / K_s$). θ_r = 0.1460 m^3 m^{-3}, θ_s = 0.4580 m^3 m^{-3}, α = 1.14 m^{-1}, n = 4.937, K_s = 0.76 m d^{-1}, and l = 0.5.

1.11 Determination of distributed soil moisture using the AHFO method

As described before, the calibration curves developed by Serna et al. (2017) were used to determine the θ profile via the AHFO method. In this section, it is provided a summary of the accuracy and precision of the DTS measurements and of the AHFO method, which allowed estimation of θ at a high-spatial resolution in the vertical direction.

The accuracy and precision of the DTS measurements were assessed using the *MB* and *RMSE*, respectively, at an integration time of 5 s. On the one hand, in the calibration sections the *MB* was of $8.1\times10^{-5} \pm 7.0\times10^{-6}$ °C and the *RMSE* was of 0.16 ± 0.01 °C (mean ± standard deviation of three repetitions), whereas in the validation section the *MB* was of -0.30 ± 0.02 °C and the *RMSE* was of 0.30 ± 0.02 °C. The values of these calibration metrics are in agreement with those reported by Hausner et al. (2011). It is important to highlight that when calculating the T_{cum}, the accuracy (*MB*) does not affect the determination of θ because these estimations are referred to the initial temperature profile in the soil. Moreover, since the T_{cum} is the integral of a temperature difference, the precision (*RMSE*) of the DTS measurements should decrease with the square root of the integration time (Selker et al, 2006a; Sayde et al., 2010). Therefore, good calibration metrics were obtained for the application of the AHFO method.

Figure 3-2 presents the AHFO calibration curve for a 20-min heat pulse and when the electric current was of ~17.5 A (which corresponds to 2.4 W m^{-1}). A comparison between the T_{cum} obtained at the saturated zone and those from the unsaturated zone demonstrates that the increase of T_{cum} is higher for lower values of θ. Also, the calibration curve has a decreasing slope as the T_{cum} increases. This behavior indicates that exists a decrease in the sensitivity of the T_{cum}–θ relation at higher water contents, which is consistent with the findings of previous studies (Sayde et al., 2010, 2014; Striegl & Loheide, 2012; Benitez-Buelga et al., 2014; 2016) and with the theoretical aspects related to Eq. (2.6).

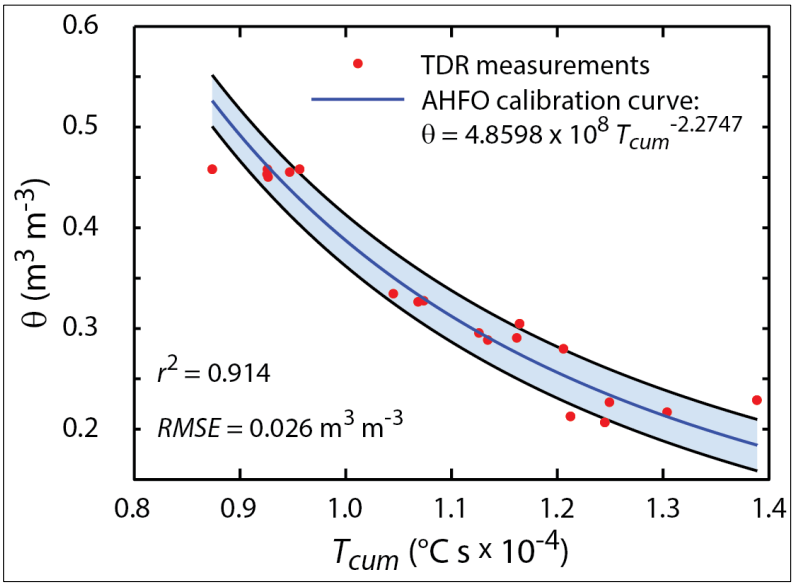

Figure 3-2: AHFO calibration curve used to determine θ. The shaded area corresponds to the calibration curve ± *RMSE* between the θ estimated via the AHFO method and the TDR sensors. This calibration curve was obtained when a current of 17.5 A (2.4 W m^{-1}) flowed through the fiber-optic cable for 20 min.

A comparison between the θ profile estimated with the AHFO method and the TDR sensors is presented in Figure 3-3. The manufactures' specifications of the TDR sensors establish that the uncertainty associated to the sensors is around 5-10% of the measurements, depending on the soil type. In this study, it is assumed a TDR error of 5% of the measurement. It can be seen in Figure 3-3 (a) that the AHFO method determines θ values with *RMSE*'s slightly larger than the errors associated to the TDR sensors' measurements. From this experience, the *RMSE* = 0.026 m^3 m^{-3} and r^2 = 0.91. The AHFO method was validated with repetitions under different hydraulic conditions. First, the AHFO calibration curve was validated at a hydraulic condition where the water table was at 1.20 m depth (Figure 3-3 (b)). Then, the performance of the AHFO method was assessed when the groundwater table depth was of 0.9 m (Figure 3-3 (c)). Small differences are observed between the estimated θ profile at the calibration experience and those obtained at the validation experiences. Errors of 0.040 m^3 m^{-3} were estimated in the validation repetition that had the groundwater level at 1.2 m depth, whereas errors

of 0.080 m^3 m^{-3} were found when the groundwater level was set to a depth of 0.9 m. These errors can be attributed to slight variations in the electrical current (on the order of ~4%), and highlights the importance of maintaining a constant electrical current when applying the AHFO method. Recent research supports the feasibility of using the AHFO method to determine θ, with errors up to 0.023 m^3 m^{-3} at θ = 0.09 m^3 m^{-3} (Benítez-Buelga et al., 2014; 2016). Observed errors can be diminished as the DTS technology advances. For instance, Sayde et al. (2014) observed that errors due to instrumentation were reduced considerably from 0.11 to 0.03 m^3 m^{-3} at saturation when a DTS instrument with better performance was employed. These errors can also be reduced if calibration of the AHFO method accounts for soil heterogeneities (Sayde et al., 2014; Benítez-Buelga, 2016), and if the effects of cable spacing and jacket configurations on accuracy are quantified (Benítez-Buelga, 2014). As the errors of the AHFO method are reduced, the method presented herein for the evaporation rate estimation can be feasible, due to the inherent relevance of the accuracy and precision on the θ measurements. In addition, the spatial scales of the AHFO method obtained in this work (~6.5 mm) are a great advantage of DTS systems. For example, the monitoring of a detailed θ profile offers the advantage of indicating the existence of high θ gradients, which could suggest changes in the soil texture, mineralogy or density.

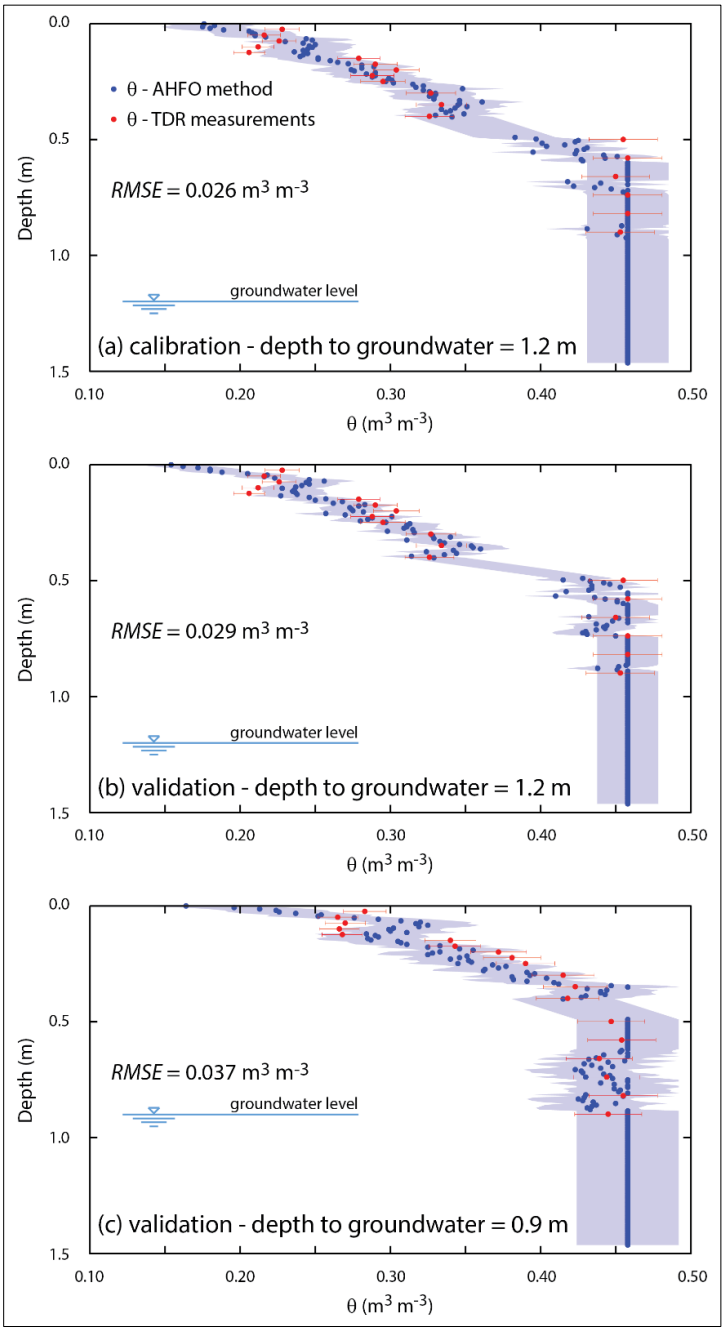

Figure 3-3: Moisture profile obtained with the AHFO method for a 20-min heat pulse: (a) θ profile used to calibrate the AHFO method. The depth to the groundwater table was of 1.2 m; (b) θ profile obtained in a repetition of the experiment when the groundwater table was at a depth of 1.2m; (c) θ profile obtained in a repetition of the experiment when the groundwater table was at a depth of 0.9m. The shaded areas correspond to the

AHFO error calculated as the RMSE between the estimated data and the TDR data. The error of the TDR sensors was assumed to be 5% of the measurement (as specified by the manufacturer).

1.12 Determination of evaporation fluxes using numerical modeling

The simulated θ profiles for different evaporation rates, as well as the experimental θ profile obtained in the soil column experiments (when the evaporation rate was 2.2 m d^{-1}) are presented in Figure 3-4. The simulated θ profiles are based on the experimental soil hydrodynamic properties (Figure 3-1). The θ profile determined through the AHFO method shows a slightly different behavior than the simulated θ profile, especially at the soil surface and at the capillary fringe. At the vicinity of the soil surface, the model results in higher moisture contents compared to the experimental data, which shows values near the residual water content. Between 0.2 and 0.6 m depth, the model has a good agreement with the experimental data. At the capillary fringe, the model underestimates the θ. This underestimation is most likely due to the shape of the van Genuchten (1980) WRC, but it may also be a result of a different density of the soil in the column compared to the density of the soil samples used to determine the experimental WRC. It was also tested the Brook and Corey's (1964) model and even when the shape of the θ profile was better represented at the capillary fringe, the shape of the θ profile was not well represented in the drier portions of the WRC. Hence, it was maintained the formulation based on the van Genuchten (1980) WRC, which provides a better description of the water retention characteristics under most circumstances (Matlan et al., 2014).

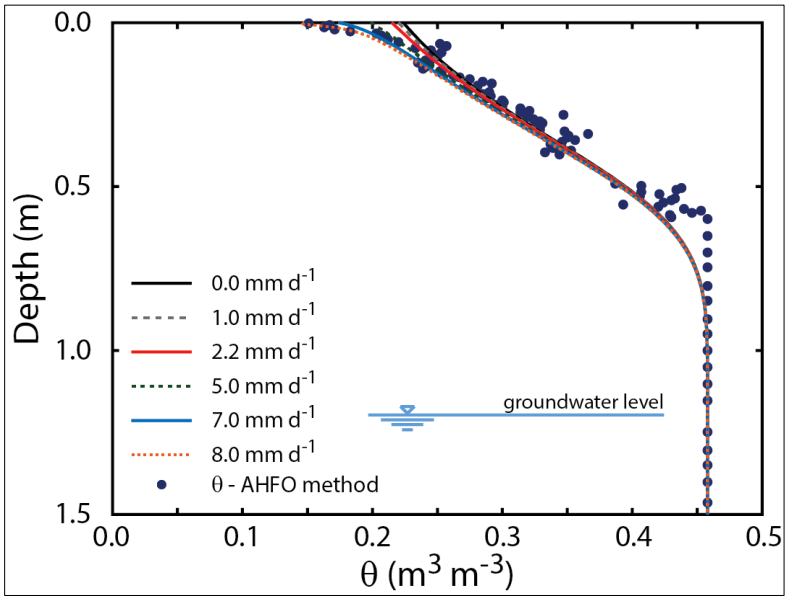

Figure 3-4: AHFO θ profile and simulated θ profiles for the soil used in this study and for different evaporation rates at steady state. The groundwater table is located at 1.2 m depth. The simulated θ profiles assume that the experimental WRF and HCF are representative of the soil packed in the column.

A sensitive analysis of the impact of the evaporation rates on the simulated θ is also shown in Figure 3-4. When the evaporation rate is zero, the θ profile takes the exact shape of the WRC, where the h profile resembles the hydrostatic pressure. As the evaporation rate increases, the θ profile changes in a subtle way in the first ~0.4 m of the soil profile. When increasing the evaporation rate in 1 mm d^{-1}, the θ at the soil surface decreases between 0.00 and 0.03 m m^{-3}. Because the AHFO method has *RMSE*'s of 0.026 m m^{-3}, it is challenging to precisely determine the evaporation rates using this methodology. Moreover, for evaporation rates equal or higher than 8 mm d^{-1}, the simulated θ profile remains constant and is no longer affected by the magnitude of the evaporation rate. Therefore, evaporation rates higher than this threshold cannot be assessed. This limitation is most likely the result of neglecting the vapor pressure gradient within the soil profile. Additionally, since evaporation is associated with an important heat removal at the surface, this limitation could be overcome by coupling the

water and heat transport in the porous media and incorporating the thermal energy balance equation at the soil surface (Assouline et al., 2013). Therefore, it is expected that a numerical model that consider liquid and water vapor transport under non-isothermal conditions, such as that of Hernández-López et al. (2016), can be used to simultaneously fit the temperature and θ profiles to produce most precise results when the threshold on the evaporation rates is surpassed. Nonetheless, it is important to note that the precision of the evaporation estimates obtained in this work, i.e., when combining the AHFO method with numerical simulations, is similar to that reported in other study that used TDR to determine evaporation rates (Plauborg, 1995). According to Schelde et al. (2011), TDR evaporation estimates constitute a lower limit of evaporation during a 24-h cycle. Furthermore, other evaporation measurement technologies, such as lysimeters, scintillometers and eddy covariance systems, also have limitations – even when some of these systems are known to have a high precision (Savage et al., 2004; Li et al., 2008; Savage, 2009).

Figure 3-5 presents a sensitivity analysis for different depths to groundwater and soil types, where the evaporation rate was increased from zero until a maximum limit (or threshold) in which no further changes in the simulated θ profile were observed. Recall that when the evaporation rate is zero, the θ profile resembles the WRC. In general, small changes on the simulated θ profile were obtained, most likely due to the hydraulic connection between the groundwater table and the soil surface. As evaporation increases, the largest changes in θ occur at the soil surface, and the water deficit at this location is supported by capillary forces that lift water from the groundwater reservoir, which acts as an infinite water source (Scherer, 1990). When the maximum evaporation limit is surpassed, the simulated θ profile does not change anymore, suggesting that the assumptions of negligible energy and vapor transfer processes, as well as the existence of a hydraulic connection between the groundwater table and the soil surface, are no longer valid. When the groundwater table was located at 0.6 m depth, the sensitivity of the sand was only 0.0005 m^3 m^{-3} for every additional millimeter of evaporated water per day. This sensitivity increased up to 0.009 m^3 m^{-3} per 1 mm d^{-1} of evaporated water

when the groundwater table was at 1.2 m depth. Therefore, for coarse-textured soils is arduous to determine the correct evaporation rate when only fitting the simulated θ profile. Nonetheless, for fine-textured soils, e.g., loam and clay, the sensitivity of the θ profile to changes in the evaporation rate varies between 0.051 and 0.098 m^3 m^{-3} per 1 mm d^{-1} of evaporated water (for the different depths to groundwater). These sensitivities can be resolved using the AHFO method (Serna et al., 2017; Sayde et al., 2014; Benítez-Buelga et al., 2014; 2016; Gil-Rodríguez, 2013). Hence, the proposed methodology should yield better results than those presented here in fine-textured soils. On one hand, the results show that as the water table is deeper and when the evaporation rate increases, the sensitivity of the θ profile increases. On the other hand, when the soil texture is coarser, this sensitivity is smaller.

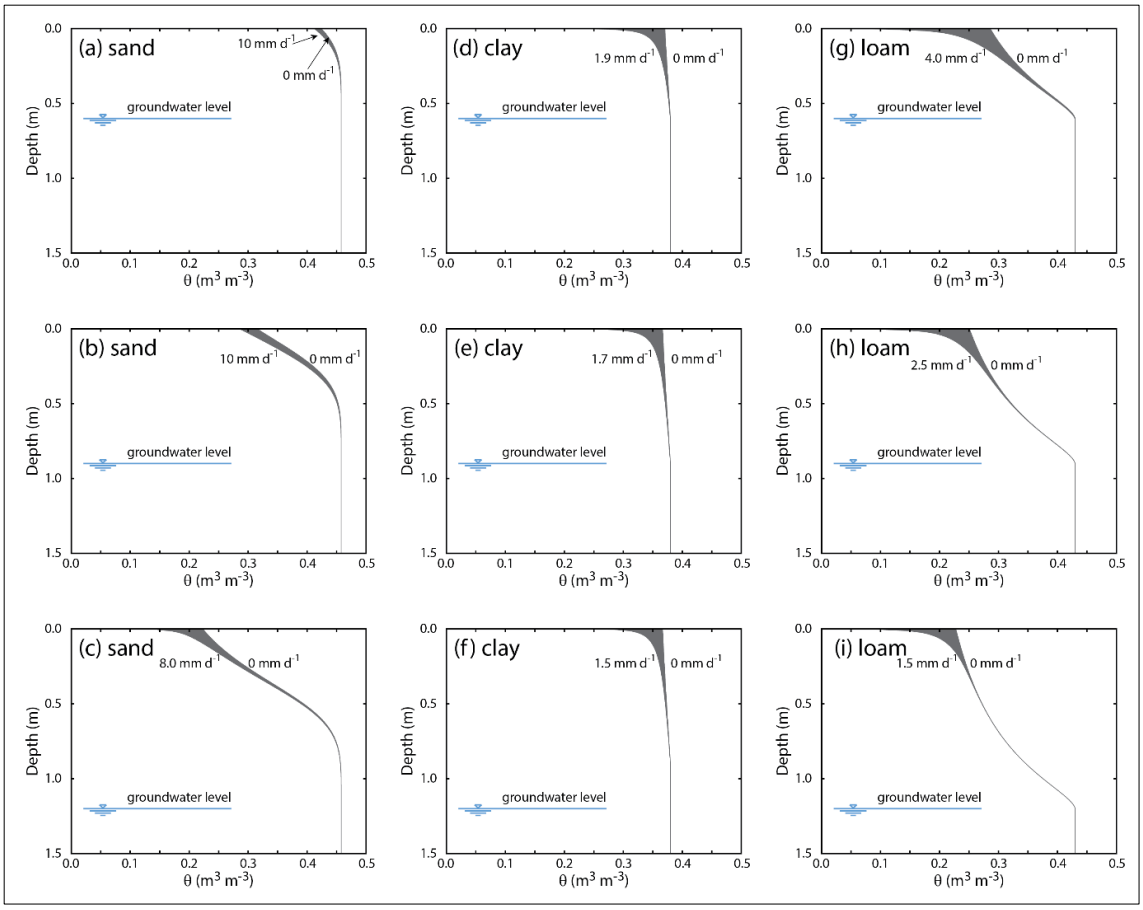

Figure 3-5: Simulated θ profiles for different soil types, evaporation rates and depths to groundwater: sand with groundwater table at depths of 0.6 m (a), 0.9 (b), and 1.2 m (c); clay with groundwater table at depths of 0.6 m (d), 0.9 m (e), and 1.2 m (f); and loam with groundwater table at depths of 0.6 m (g), 0.9 m (h), and 1.2 m (i).

To further investigate the impact of the hydrodynamic parameters on the simulated θ profile, another sensitivity analysis was carried out. In this analysis, which is shown in Figure 3-6, the experimental evaporation rate was maintained at 2.2 mm d^{-1}, while the θ_r, α, n, K_s and l parameters were varied. Figure 3-6 also shows how the WRC and HCF change as the hydrodynamic parameters are changed. As expected, when the θ_r decreases, the θ simulated at the soil surface decreases, and the main changes in the hydrodynamic properties occur at the lowest moisture contents (Figure 3-6 (a)). When θ_r

diminishes, the simulated θ at the soil surface agrees better with the corresponding experimental data. Nevertheless, the slope of the simulated θ profile differs from the measured θ at most of the unsaturated zone. The van Genuchten (1980) model typically has poor results at low moisture contents. Therefore, it is important to improve the representation of the WRC at the drier portions of the curve (Nimmo, 1991). Changes in α values result in important variations in the simulated θ profile and in the WRC, but no changes in the HCF (Figure 3-6 (b)). Given the large sensitivity of the θ profile to this parameter, it is important to correctly characterize α when obtaining the WRC at the laboratory. On the other hand, finding a correct value for *n* is more difficult due to its nature of being a fitting parameter. Even when the WRC and the HCF show a low sensitivity to the *n* parameter, the simulated θ profile displays a more relevant variation. In this case, an increase in *n* results in a better agreement between the simulated and experimental θ profiles, as well as a better agreement at the vicinity of the soil surface and at the capillary fringe (Figure 3-6 (c)). The effects of the variations of K_s and *l* on the θ profile are shown in Figure 3-6 (d) and (e). Only the θ profile at the vicinity of the soil surface is affected when the previous parameters are varied. A reduction of the K_s and an increase in *l* result in a better agreement between the simulated and measured θ near the soil surface. Since these parameters are used to estimate the HCF, reliable estimates of them are needed to improve the methodology proposed in this work. Nonetheless, the experimental determination of the HCF is more difficult than that of the WRC (Assouline & Or, 2013).

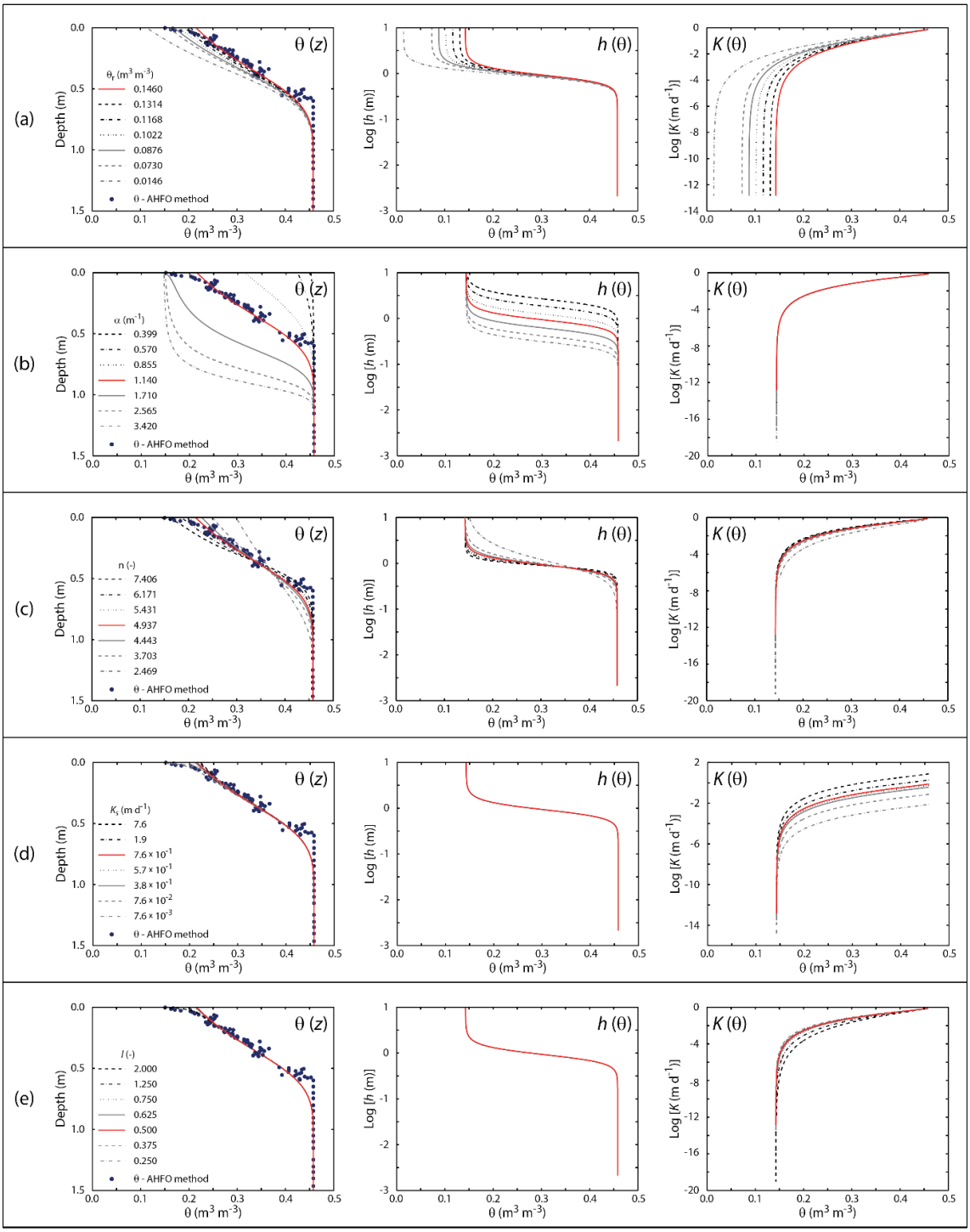

Figure 3-6: Sensitivity analysis of the θ profile, $h(\theta)$ and $K(\theta)$ when the following parameters are varied: θ_r (a), α (b), n (c), K_s (d), and l (e). The groundwater table is located at 1.2 m depth.

Monte Carlo simulations were carried out to assess the uncertainty between all the hydrodynamic properties and their effect on the simulated θ profile. To this end, these properties were first fitted to have a best agreement between the simulated and experimental θ profile (using the experimental evaporation rate of 2.2 m d^{-1}), and then the Monte Carlo simulations were performed (200 runs). The fitting process was used as a means to define the input parameters of the Monte Carlo simulations (as explained below).

The θ_s and K_s were fixed to their experimental values, and θ_r, α, n and l were fitted using the Hydrus 1D's inverse modeling mode. Figure 3-7(a) shows the fitted θ profile, where it can be seen that the simulation using the fitted parameters represents better the θ profile in the unsaturated zone, compared to the results obtained with the hydrodynamic parameters estimated in the laboratory. In the capillary fringe, the θ is underestimated by both simulations, but the results with the fitted parameters show a slight improvement. The third column of Table 3-1(μ) presents the fitted hydrodynamic properties. On one hand, the fitted θ_r and α, differs in less than 4% of the experimental estimates, and n increases only in an 11%. On the other hand, the pore-connectivity parameter, l, showed the most significant variation, increasing from 0.5 to 1.622. Figure 3-7 (b) and (c) portray the resulting WRC and HCF, and reveals that the WRC was not affected by the fitting process. However, the HCF suffered major changes because of the great increase in l.

Table 3-1: Parameters used in the Monte Carlo simulations. All the probability density distributions were assumed to follow ~N(μ,σ).

Parameter	**Units**	μ	σ
$\boldsymbol{\theta_s}$	$\mathbf{m^3\ m^{-3}}$	0.458	0.011
$\boldsymbol{\theta_r}$	$\mathbf{m^3\ m^{-3}}$	0.143	0.022
$\boldsymbol{\alpha}$	$\mathbf{m^{-1}}$	1.094	0.023
$\boldsymbol{n}$	-	5.473	0.420

K_s	**m d^{-1}**	0.560	0.350
l	-	1.622	0.360

To define the probability distributions of each input parameter in the Monte Carlo simulations, it was assumed that the hydrodynamic properties follow a normal distribution with mean μ and standard deviation σ. These parameters were obtained from the inverse simulations carried out in Hydrus 1D and are presented in Table 3-1. Figure 3-7 (d) shows the results of the Monte Carlo simulations (gray lines), and the θ profiles associated to an error of ± 0.05 m^3 m^{-3} (green lines) with respect to the fitted θ profile (light blue line). These results highlight that a larger uncertainty is expected near the soil surface, where the Monte Carlo analysis shows errors larger than ± 0.05 m^3 m^{-3}. Figure 3-7 (e) and (f) present the variability of the WRC and the HCF that resulted from these simulations. At soil water contents near 0.3 m^3 m^{-3}, the 200 simulated WRC's (Figure 3-7 (e)) show fewer deviations from the fitted WRC. The 200 HCF's (Figure 3-7 (f)) increase their difference with the fitted HCF as the θ decreases. At the first 0.1 m in the soil profile, an *RMSE* of 0.023 m^3 m^{-3} occurs between the Monte Carlo simulations and the fitted θ profile. As shown in Table 3-2, the *RMSE* decreases at deeper depths. The *RMSE* in the soil profile that has a θ smaller than saturation, i.e., between 0 and 0.80 m depth, is of 0.015 m^3 m^{-3}, and the overall RMSE all along the soil profile, i.e., between 0 and 1.50 m depth, is of 0.013 m^3 m^{-3}. Since greater errors are associated to the zone near the soil surface, a better precision is required to determine the θ profile that can yield successful estimations of the evaporation rates.

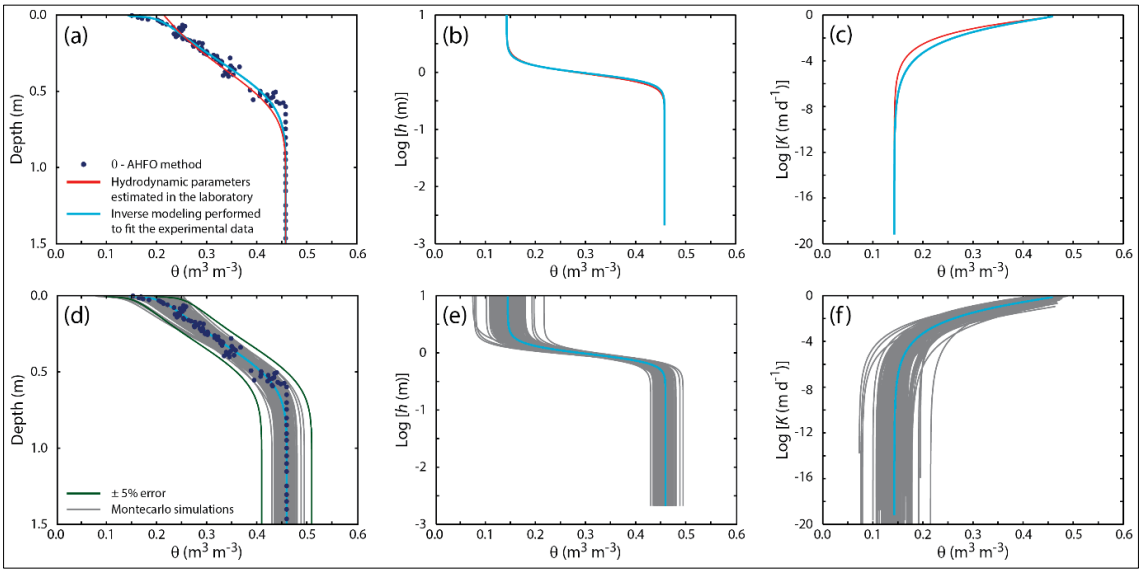

Figure 3-7: θ profile (a), $h(\theta)$ (b) and $K(\theta)$ (c) for the soil used in this study when the van Genuchten parameters are optimized to fit the simulated θ profile to the experimental data. The optimized hydrodynamic parameters are: θ_r = 0.1429 m^3 m^{-3}, θ_s = 0.4580 m^3 m^{-3}, α = 1.0940 m^{-1}, n = 5.473, K_s = 0.76 m d^{-1}, and l = 1.622. θ profile (d), $h(\theta)$ (e) and $K(\theta)$ (f) showing the results of the Monte Carlo simulations.

Despite the good agreement between the predicted and the measured moisture in the sandy soil packed in the laboratory column, difficulties arose in the course of this research. These difficulties are mainly due to the requirement of high accuracy and precision for the evaporation rate estimation and the low sensitivity of the θ profile to changes in the evaporation rate, because of the laboratory conditions imposed. Errors caused by a deficient soil heterogeneity characterization, AHFO method measurements (i.e., due to the AHFO calibration curve used in this study), and hydraulic parameters estimation should be minimized. Additionally, due to the importance of having a good characterization of the θ profile at the vicinity of the soil surface, it is important to estimate precisely the soil hydrodynamic properties – especially the HCF since it has an important impact in the moisture content at the soil surface. Nonetheless, the spatial scales of the AHFO method utilized in this work (~6.5 mm) are a great advantage of

DTS system that should be further explored to improve the analysis presented in this work.

Table 3-2: *RMSE* of the Monte Carlo simulations as a function of depth.

Depth (m)	***RMSE*** **(m^3 m^{-3})**
0.00 – 0.10	0.023
0.10 – 0.20	0.012
0.20 – 0.30	0.008
0.30 – 0.40	0.007
0.40 – 0.50	0.006
0.50 – 0.60	0.005
0.60 – 0.70	0.005
0.70 – 0.80	0.004
0.80 – 0.90	0.004
0.00 – 0.80	0.015
0.00 – 1.50	0.013

4. CONCLUSIONS AND PERSPECTIVES

In this work, it was proposed a method to determine evaporation rates by combining the AHFO method with numerical modeling, for conditions of negligible vapor pressure gradient and negligible water flow due to thermal gradients within the soil profile, which typically occur when the groundwater table is shallow. This method requires assessing the soil hydrodynamic properties beforehand. Therefore, the experimental soil WRC and HCF were determined. Then, soil column experiments were carried out to assess this method. In the soil column experiments, the groundwater table was fixed, evaporation was monitored with a precision of ± 0.1 mm d^{-1}, and a vertical high-resolution FO-DTS system measured the thermal profile with a spatial resolution of ~6.5 mm. The fiber-optic cable had conductive elements that permitted application of the AHFO method. Finally, the experimental θ profile –obtained with the AHFO method– was used in the numerical simulations to determine if evaporation rates could be determined by inverse modeling.

It was found that the accuracy (-0.30 ± 0.02 °C) and precision (0.30 ± 0.02 °C) of the DTS system –when the DTS traces were obtained at 5 s integration intervals– were appropriate for the application of the AHFO method using 20-min heat pulses. The error associated to the θ estimates was of ~0.026 m^3 m^{-3} (r^2 = 0.91). The soil WRC and HCF –based on laboratory data– were used to find numerically the θ profile under the same conditions tested in the soil column experiments. The numerical model provided a slightly different behavior than the experimentally measured θ profile, especially at the soil surface and at the capillary fringe.

A sensitivity analysis showed that as the evaporation rate increased, the θ profile changed in a subtle way in the first ~0.4 m. For evaporation rates higher than a specific threshold, which depends on the groundwater table depth and on the soil type, the simulated θ profile is no longer affected by the magnitude of the evaporation rate. Therefore, evaporation rates higher than this threshold cannot be assessed. This

limitation is most likely the result of neglecting the vapor pressure gradient within the soil profile, and could be overcome by coupling the water and heat transport in the porous media and incorporating the surface energy balance. As in the experiments and numerical runs the θ at the soil surface was not very sensitive to changes in the evaporation rate, especially in coarse-textured soils, to improve the evaporation estimates, more precision is required on the representation of the soil hydrodynamic properties, the soil heat-vapor-water dynamics, and the measured θ at the soil surface.

It was also found that the laboratory estimates of θ_r, α, n and K_s were very close to those that results in a good agreement between experimental and simulated θ profiles. However, it should be pointed out that finding a correct value for the n parameter may be difficult due to its nature of being a fitting parameter. Contrarily, the l parameter greatly influences the HCF, and even when it does not affects the WRC, variations in l results in important fluctuations on the θ profile near the soil surface. In the experiments, the l parameter that resulted in the best match between experimental and simulated θ profiles, varied in more than 200% from the suggested value proposed by Mualem (1976).

As the uncertainty analysis showed that the greater errors occur near the soil surface, a better precision is required when determining the hydrodynamic parameters that result in greater variations of the moisture content at this location of the soil profile, i.e., α, n and l. Additionally, improvements in the AHFO calibration curve can reduce the errors of the estimated θ profile, which can yield successful estimations of the evaporation rates for a wider range of soil textures. Nonetheless, it should be emphasized that the spatial scales achieved with the AHFO method (6.5 mm) are an important advantage of the proposed method that should be further explored to improve the analysis presented in this work.

REFERENCES

Assouline, S., and D. Or (2013), Conceptual and parametric representation of soil hydraulic properties: A review, *Vadose Zone J., 12*(4), doi:10.2136/vzj2013.07.0121.

Assouline, S., S. W. Tyler, J. S. Selker, I. Lunati, C. W. Higgins, and M. B. Parlange (2013), Evaporation from a shallow water table: Diurnal dynamics of water and heat at the surface of drying sand, *Water Resour. Res., 49*(7), 4022-4034, doi:10.1002/wrcr.20293.

Assouline, S., K. Narkis, R. Gherabli, P. Lefort, and M. Prat (2014), Analysis of the impact of surface layer properties on evaporation from porous systems using column experiments and modified definition of characteristic length, *Water Resour. Res., 50*(5), 3933-3955, doi:10.1002/2013WR014489.

Bastidas-Oyanedel, J. R., C. Fang, S. Almardeai, U. Javid, A. Yousuf, and J. E. Schmidt (2016), Waste biorefinery in arid/semi-arid regions, *Bioresour. Technol., 215*, 21-28, doi: 10.1016/j.biortech.2016.04.010.

Benítez-Buelga, J., C. Sayde, L. Rodríguez-Sinobas, and J. S. Selker (2014), Heated fiber optic distributed temperature sensing: A dual-probe heat-pulse approach, *Vadose Zone J., 13*(11), doi:10.2136/vzj2014.02.0014.

Benítez-Buelga, J., L. Rodríguez-Sinobas, R. Sánchez-Calvo, M. Gil-Rodríguez, C. Sayde, and J. S. Selker (2016), Calibration of soil moisture sensing with subsurface heated fiber optics using numerical simulation, *Water Resour. Res., 52*(4), 2985-2995, doi:10.1002/2015WR017897.

Bristow, K. L., R. D. White, and G. J. Kluitenberg (1994), Comparison of single and dual probes for measuring soil thermal properties with transient heating, *Soil Res., 32*(3), 447-464, doi:10.1071/SR9940447.

Brooks, R. H., and A. T. Corey (1964), Hydraulic properties of porous media and their relation to drainage design, *Trans. ASAE, 7*(1), 0026-0028, doi:10.13031/2013.40684.

Cai, W., T. Cowan, and M. Thatcher (2012), Rainfall reductions over Southern Hemisphere semi-arid regions: the role of subtropical dry zone expansion, *Sci. Rep.-UK, 2*, 702, doi:10.1038/srep00702.

Campbell, G. S., C. Calissendorff, and J. H. Williams (1991), Probe for measuring soil specific heat using a heat-pulse method, *Soil Sci. Soc. Am. J., 55*(1), 291-293, doi:10.2136/sssaj1991.03615995005500010052x.

Campbell, N. R. (2013), *Physics: the elements*, New York: Cambridge University Press.

Ciocca, F., I. Lunati, N. Van de Giesen, and M. B. Parlange (2012), Heated optical fiber for distributed soil-moisture measurements: A lysimeter experiment, *Vadose Zone J., 11*(4), doi:10.2136/vzj2011.0199.

Cristi, F., V. Fierro, F. Suárez, J. F. Muñoz, and M. B. Hausner (2016), A TDR-waveform approach to estimate soil water content in electrically conductive soils, *Comput. Electron. Agr., 121*, 160-168, doi:10.1016/j.compag.2015.12.004.

De Vries, D. A. (1958), Simultaneous transfer of heat and moisture in porous media, *Eos Trans. AGU, 39*(5), 909-916, doi:10.1029/TR039i005p00909.

De Vries, D. A., and A. J. Peck (1958), On the cylindrical probe method of measuring thermal conductivity with special reference to soils. I. Extension of theory and discussion of probe characteristics, *Aust. J. Phys., 11*(2), 255-271, doi: 10.1071/PH580255.

Desilets, D., M. Zreda, and T. P. A. Ferré (2010), Nature's neutron probe: Land surface hydrology at an elusive scale with cosmic rays, *Water Resour. Res., 46*(11), W11505, doi: 10.1029/2009WR008726.

Dong, J., S. C. Steele-Dunne, T. E. Ochsner, and N. van de Giesen (2015), Determining soil moisture by assimilating soil temperature measurements using the Ensemble Kalman Filter, *Adv. Water Resour., 86*, 340-353, doi: 10.1016/j.advwatres.2015.08.011.

Dong, J., S. C. Steele-Dunne, T. E. Ochsner, and N. van de Giesen (2016), Estimating soil moisture and soil thermal and hydraulic properties by assimilating soil temperatures

using a particle batch smoother, *Adv. Water Resour., 91*, 104-116, doi:10.1016/j.advwatres.2015.08.011.

Gil-Rodríguez, M., L. Rodríguez-Sinobas, J. Benítez-Buelga, and R. Sánchez-Calvo (2013), Application of active heat pulse method with fiber optic temperature sensing for estimation of wetting bulbs and water distribution in drip emitters, *Agr. Water Manage., 120*, 72-78, doi:10.1016/j.agwat.2012.10.012.

Griffiths, D. J. (2008), Electrodynamics, in Introduction to Electrodynamics, *Pearson Benjamin Cummings*, San Francisco, CA, 285-342.

Hausner, M. B., F. Suárez, K. E. Glander, N. van de Giesen, J. S. Selker, and S. W. Tyler (2011), Calibrating single-ended fiber-optic Raman spectra distributed temperature sensing data, *Sensors, 11*(11), 10859-10879, doi:10.3390/s111110859.

Hausner, M. B., and S. Kobs (2016), Identifying and correcting step losses in single-ended fiber-optic distributed temperature sensing data, *J. Sensors*, *2016*, 10, doi:10.1155/2016/7073619.

Hernández-López, M. F., J. Gironás, I. Braud, F. Suárez, and J. F. Muñoz (2014), Assessment of evaporation and water fluxes in a column of dry saline soil subject to different water table levels, *Hydrol. Process., 28*(10), 3655-3669, doi:10.1002/hyp.9912.

Hernández-López, M. F., I. Braud, J. Gironás, F. Suárez, and J. F. Muñoz (2016), Modelling evaporation processes in soils from the Huasco salt flat basin, Chile, *Hydrol. Process., 30*(25), 4704-4719, doi: 10.1002/hyp.10987.

Intergovernmental Panel On Climate Change (2007), Climate change 2007: impacts, adaptation and vulnerability, *IPCC WGII Fourth Assessment Report*.

Jury, W. A., and R. Horton (2004), *Soil physics*, John Wiley & Sons.

Klute, A. (1994), Methods of soil analysis, part 1: physical and mineralogical methods, *Agronomy Series, 9*, American Society of Agronomy, Madison, Wisconsin.

Kurth, A. M., N. Dawes, J. Selker, and M. Schirmer (2013), Autonomous distributed temperature sensing for long-term heated applications in remote areas, *Geosci. Instrum. Meth., 2*(1), 71-77, doi:10.5194/gi-2-71-2013.

Li, S., S. Kang, F. Li, and L. Zhang (2008), Evapotranspiration and crop coefficient of spring maize with plastic mulch using eddy covariance in northwest China, *Agr. Water Manage., 95*(11), 1214-1222, doi:10.1016/j.agwat.2008.04.014.

Li, M., B. C. Si, W. Hu, and M. Dyck (2016), Single-Probe Heat Pulse Method for Soil Water Content Determination: Comparison of Methods, *Vadose Zone J., 15*(7), doi:10.2136/vzj2016.01.0004.

Luxemburg, W., T. Euser., C. Everson, M. Mengistu, W. Bastiaanssen, and A. Clulow (2013), A new method to measure bowen ratios using high resolution vertical dry and wet bulb temperature profiles, Hydrology and Earth System Sciences Discussions, 10 (6).

Euser, T., W. M. J. Luxemburg, C. S. Everson, M. G. Mengistu, A. D. Clulow, and W. G. M. Bastiaanssen (2014), A new method to measure Bowen ratios using high-resolution vertical dry and wet bulb temperature profiles, *Hydrol. Earth Syst. Sci*., *18*, 2021-2032, doi:10.5194/hess-18-2021-2014.

Marek, G., P. Gowda, T. Marek, B. Auvermann, S. Evett, P. Colaizzi, and D. Brauer (2016), Estimating preseason irrigation losses by characterizing evaporation of effective precipitation under bare soil conditions using large weighing lysimeters, Agricultural Water Management, 169, 115-128.

Matlan, S. J., M. Mukhlisin, and M. R. Taha (2014), Performance evaluation of four-parameter models of the soil-water characteristic curve, *Sci. World J., 2014*, 12, doi:10.1155/2014/569851.

McJannet, D. L., F. J. Cook, R. P. McGloin, H. A. McGowan, and S. Burn (2011), Estimation of evaporation and sensible heat flux from open water using a large-aperture scintillometer, *Water Resour. Res., 47*(5), W05545, doi:10.1029/2010WR010155.

Millennium Ecosystem Assessment (2005), Current state and trends, *Washington, DC*.

Mills, A. F. (1999), *Basic heat and mass transfer,* Pearson College Div.

Moene, A. F., and J. C. van Dam (2014), *Transport in the atmosphere-vegetation-soil continuum,* New York: Cambridge University Press.

Mualem, Y. (1976), A new model for predicting the hydraulic conductivity of unsaturated porous media, *Water Resour. Res., 12*(3), 513-522, doi:10.1029/WR012i003p00513.

Nasrallah, S. B., and P. Perre (1988), Detailed study of a model of heat and mass transfer during convective drying of porous media, *Int. J. Heat Mass Tran., 31*(5), 957-967, doi:10.1016/0017-9310(88)90084-1.

Nimmo, J. R. (1991), Comment on the treatment of residual water content in "A consistent set of parametric models for the two-phase flow of immiscible fluids in the subsurface" by L. Luckner et al., *Water Resour. Res., 27*(4), 661-662, doi:10.1029/91WR00165.

Ortiz, C., R. Aravena, E. Briones, F. Suárez, C. Tore, and J. F. Muñoz (2014), Sources of surface water for the Soncor ecosystem, Salar de Atacama basin, northern Chile, *Hydrolog. Sci. J., 59*(2), 336-350, doi:10.1080/02626667.2013.829231.

Parlange, M. B., A. T. Cahill, D. R. Nielsen, J. W. Hopmans, and O. Wendroth (1998), Review of heat and water movement in field soils, *Soil Till. Res., 47*(1), 5-10, doi:10.1016/S0167-1987(98)00066-X.

Peters, A., and W. Durner (2008), Simplified evaporation method for determining soil hydraulic properties, *J. Hydrol., 356*(1), 147-162, doi:10.1016/j.jhydrol.2008.04.016.

Plauborg, F. (1995), Evaporation from bare soil in a temperate humid climate—measurement using micro-lysimeters and time domain reflectometry, *Agr. Forest Meteorol., 76*(1), 1-17, doi:10.1016/0168-1923(94)02215-6.

Prat, M. (2002), Recent advances in pore-scale models for drying of porous media, *Chem. Eng. J., 86*(1), 153-164, doi:10.1016/S1385-8947(01)00283-2.

Rawls, W. J., D. L. Brakensiek, and K. E. Saxtonn (1982), Estimation of soil water properties, *T. ASAE, 25*(5), 1316-1320, doi:10.13031/2013.33720.

Ren, T., T. E. Ochsner, and R. Horton (2003), Development of thermo-time domain reflectometry for vadose zone measurements. *Vadose Zone J., 2*(4), 544-551, doi:10.2136/vzj2003.5440.

Richards, L. A. (1931), Capillary conduction of liquids through porous mediums, *J. Appl. Phys., 1*(5), 318-333, doi:10.1063/1.1745010.

Ruskowitz, J. A., F. Suárez, S. W. Tyler, and A. E. Childress (2014), Evaporation suppression and solar energy collection in a salt-gradient solar pond, *Sol. Energy, 99*, 36-46, doi:10.1016/j.solener.2013.10.035.

Sandoval, V., C. A. Bonilla, J. Gironás, S. Vera, F. Victorero, W. Bustamante, V. Rojas, E. Leiva, P. Pastén, and F. Suárez (2017), Porous Media Characterization to Simulate Water and Heat Transport through Green Roof Substrates, *Vadose Zone J., 16*(4), doi:10.2136/vzj2016.10.0101.

Savage, M. J., C. S. Everson, G. O. Odhiambo, M. G. Mengistu, and C. Jarmain (2004), Theory and practice of evaporation measurement, with special focus on surface layer scintillometry as an operational tool for the estimation of spatially averaged evaporation, *Water Res. Commission Report* (1335/1), 04.

Savage, M. J. (2009), Estimation of evaporation using a dual-beam surface layer scintillometer and component energy balance measurements, *Agr. Forest Meteorol., 149*(3), 501-517, doi:10.1016/j.agrformet.2008.09.012.

Sayde, C., C. Gregory, M. Gil-Rodríguez, N. Tufillaro, S. Tyler, N. van de Giesen, M. English, R. Cuenca, and J. S. Selker (2010), Feasibility of soil moisture monitoring with heated fiber optics, *Water Resour. Res., 46*(6), W06201, doi:10.1029/2009WR007846.

Sayde, C., J. B. Buelga, L. Rodriguez-Sinobas, L. E. Khoury, M. English, N. van de Giesen, and J. S. Selker (2014), Mapping variability of soil water content and flux across 1–1000 m scales using the Actively Heated Fiber Optic method, *Water Resour. Res., 50*, 1702-7317, doi:10.1002/2013WR014983.

Schelde, K., R. Ringgaard, M. Herbst, A. Thomsen, T. Friborg, and H. Sogaard (2011), Comparing evapotranspiration rates estimated from atmospheric flux and TDR soil moisture measurements, *Vadose Zone J., 10*(1), 78-83, doi: 10.2136/vzj2010.0060.

Scherer, G. W. (1990), Theory of drying, *J. Am. Ceram. Soc., 73*(1), 3-14, doi:10.1111/j.1151-2916.1990.tb05082.x.

Schilperoort, B., M. Coenders-Gerrits, W. Luxemburg, C. Cisneros-Vaca, and M. Ucer (2016), Verifying the distributed temperature sensing Bowen ratio method for measuring evaporation, *in EGU General Assembly Conference Abstracts, 18*, 84-86.

Scott, R. L. (2010), Using watershed water balance to evaluate the accuracy of eddy covariance evaporation measurements for three semiarid ecosystems, *Agr. Forest Meteorol., 150*(2), 219-225, doi:10.1016/j.agrformet.2009.11.002.

Selker, J. S., L. Thévenaz, H. Huwald, A. Mallet, W. Luxemburg, N. Van De Giesen, M. Stejskal, J. Zeman, M. Westhoff, and M. B. Parlange (2006a), Distributed fiber-optic temperature sensing for hydrologic systems, *Water Resour. Res., 42*(12), W12201, doi:10.1029/2006WR005326.

Selker, J., N. van de Giesen, M. Westhoff, W. Luxemburg, and M. B. Parlange (2006b), Fiber optics opens window on stream dynamics, *Geophys. Res. Lett., 33*(24), L24401, doi:10.1029/2006GL027979.

Serna, J. L. (2015), Evaluación del método activo para determinar contenidos de humedad en suelos *(*Master's Thesis*), Pontificia Universidad Católica de Chile, Santiago de Chile.*

Serna, J. L., F. I. Suárez, and J. F. Muñoz (2017), Evaluación del método activo para determinar contenidos de humedad en suelos, *Ingeniería del Agua, 21*(3), 165-178, doi:10.4995/ia.2017.6802.

Shokri, N., and G. Salvucci (2011), Evaporation from porous media in the presence of a water table, *Vadose Zone J., 10*(4), 1309-1318, doi:10.2136/vzj2011.0027.

Shuttleworth, W. J., M. Zreda, X. Zeng, C. Zweck, and T. P. Ferré (2010), The COsmic-ray Soil Moisture Observing System (COSMOS): a non-invasive, intermediate scale soil moisture measurement network, in *Third International Symposium, Role of hydrology managing consequences of a changing global environment. Br. Hydrol. Soc. Newcastle, England.*

Silva, C., D. González, and F. Suárez (2017), An experimental and numerical study of evaporation reduction in a salt-gradient solar pond using floating discs, *Sol. Energy, 142*, 204-214, doi:10.1016/j.solener.2016.12.036.

Šimůnek, J., M. T. van Genuchten, and M. Šejna (2016), Recent developments and applications of the HYDRUS computer software packages, *Vadose Zone J., 15*(7), doi:10.2136/vzj2016.04.0033.

Steele-Dunne, S. C., M. M. Rutten, D. M. Krzeminska, M. Hausner, S. W.Tyler, J. Selker, T. A. Bogaard, and N. C. van de Giesen (2010), Feasibility of soil moisture estimation using passive distributed temperature sensing, *Water Resour. Res., 46*(3), W03534, doi:10.1029/2009WR008272.

Striegl, A. M., I. I. Loheide, and P. Steven (2012), Heated distributed temperature sensing for field scale soil moisture monitoring, *Groundwater, 50*(3), 340-347, doi:10.1111/j.1745-6584.2012.00928.x.

Suárez, F., J. E. Aravena, M. B. Hausner, A. E. Childress, and S. W. Tyler (2011a), Assessment of a vertical high-resolution distributed-temperature-sensing system in a shallow thermohaline environment, *Hydrol. Earth Sys. Sci., 15*(3), 1081-1093, doi:10.5194/hess-15-1081-2011.

Suárez, F., M. B. Hausner, J. Dozier, J. S. Selker, and S. W. Tyler (2011b), Heat transfer in the environment: Development and use of fiber-optic distributed temperature sensing, In *Developments in Heat transfer*, Intech.

Tarara, J. M., and J. M. Ham (1997), Measuring soil water content in the laboratory and field with dual-probe heat-capacity sensors, *Agron. J., 89*(4), 535-542, doi:10.2134/agronj1997.00021962008900040001x.

Topp, G. C., J. L. Davis, and A. P. Annan (1980), Electromagnetic determination of soil water content: Measurements in coaxial transmission lines, *Water Resour. Res., 16*(3), 574-582, doi:10.1029/WR016i003p00574.

Twarakavi, N. K., J. Šimůnek and M. Schaap (2010). Can texture-based classification optimally classify soils with respect to soil hydraulics? *Water Resour. Res., 46*(1), W01501, doi:10.1029/2009WR007939.

United States Department of Agriculture (2014), *Keys to soil taxonomy* (Twelfth ed.), United States of America: Natural Resources Conservation Service.

Van Genuchten, M. T. (1980), A closed-form equation for predicting the hydraulic conductivity of unsaturated soils. *Soil Sci. Soc. Am. J., 44*(5), 892-898, doi:10.2136/sssaj1980.03615995004400050002x.

Vásquez, C., C. Ortiz, F. Suárez, and J. F. Muñoz (2013), Modeling flow and reactive transport to explain mineral zoning in the Atacama salt flat aquifer, Chile, *J. Hydrol., 490*, 114-125, doi:10.1016/j.jhydrol.2013.03.028.